Luu, T-H., Hin, R., Coath, C., & Elliott, T. (2019). Bulk chondrite variability in mass independent magnesium isotope compositions – Implications for initial solar system $^{26}Al/^{27}Al$ and the timing of terrestrial accretion. *Earth and Planetary Science Letters*, *522*, 166-175. https://doi.org/10.1016/j.epsl.2019.06.033

BULK CHONDRITE VARIABILITY IN MASS INDEPENDENT MAGNESIUM ISOTOPE COMPOSITIONS - IMPLICATIONS FOR INITIAL SOLAR SYSTEM ^{26}AL/^{27}AL AND THE TIMING OF TERRESTRIAL ACCRETION

Tu-Han Luu*, Remco C. Hin, Christopher D. Coath and Tim Elliott

Bristol Isotope Group, School of Earth Sciences, University of Bristol, Bristol BS8 1RJ, UK

* Corresponding author: tutu.luu@bristol.ac.uk

Keywords: Mg-isotope analyses, bulk chondrites, planetary bodies, ^{26}Mg mass-independent variability, ^{26}Al homogeneity.

Abstract

We have determined $\Delta'^{26}Mg_{DSM-3}$, the mass-independent variations in $^{26}Mg/^{24}Mg$, of primitive, bulk meteorites to precisions better than ± 3 ppm (2se). Our measurements of samples from 10 different chondrite groups show $\Delta'^{26}Mg_{DSM-3}$ that vary from −5 to 22 ppm. Our data define an array with a positive slope in a plot of $\Delta'^{26}Mg_{DSM-3}$ against $^{27}Al/^{24}Mg$, which can be used to determine $(^{26}Al/^{27}Al)_0$, i.e. initial $^{26}Al/^{27}Al$, and $(\Delta'^{26}Mg_{DSM-3})_0$, i.e. initial $\Delta'^{26}Mg_{DSM-3}$. On such an isochron plot, the best fit of our new measurements combined with literature data implies $(^{26}Al/^{27}Al)_0$ of (4.67±0.78)x10^{-5} and $(\Delta'^{26}Mg_{DSM-3})_0$ of −31.6 ± 5.7 ppm (2se) for ordinary and carbonaceous chondrites, other than CR chondrites, which have anomalously low $\Delta'^{26}Mg_{DSM-3}$. These parameters are within uncertainty of those defined by previous measurements of bulk calcium-, aluminium-rich inclusions (CAIs) that set canonical $(^{26}Al/^{27}Al)_0 \sim 5x10^{-5}$. The most straightforward interpretation of all these observations is that

differences in the Al/Mg of bulk ordinary and carbonaceous chondrites are dominantly controlled by variable contributions of early-formed refractory and major silicate components derived from a common, canonical reservoir. The $\Delta'^{26}Mg_{DSM\text{-}3}$ of enstatite chondrites are slightly more radiogenic (~ 3 ppm) at similar Al/Mg to the ordinary chondrites. We speculate that this is related to the timing of removal of a refractory component from the source reservoirs of these different meteorite groups; the higher $\Delta'^{26}Mg_{DSM\text{-}3}$ of the enstatite chondrites suggests later (~ 0.5 Ma post CAIs) condensation and loss of this refractory component. Despite inferred consistency of $(^{26}Al/^{27}Al)_0$ and $(\Delta'^{26}Mg_{DSM\text{-}3})_0$ across most chondrite groups, some nebular heterogeneity is required to account for the compositions of CR chondrites. Our preferred interpretation is that the CR source region has lower $(\Delta'^{26}Mg_{DSM\text{-}3})_0$. As the most appropriate isotopic reference for the Earth, our new mean enstatite chondrite composition allows us to assess possible ingrowth of ^{26}Mg from live ^{26}Al during accretion of the Earth. The Earth has $\Delta'^{26}Mg_{DSM\text{-}3}$ within uncertainty of enstatite chondrites, despite its higher Al/Mg. This requires that the terrestrial increase in Al/Mg, which we attribute to vapour loss during accretion, must have happened > 1.5 Ma post CAI formation, in an instantaneous fractionation model.

1 Introduction

The magnitude and variability of initial $^{26}Al/^{27}Al$, or $(^{26}Al/^{27}Al)_0$, in the solar protoplanetary disk (hereafter SPD) is of great importance for its setting and dynamics, ^{26}Al-^{26}Mg chronometry and the melting of planetesimals. Magnesium isotope measurements of the oldest, dated solar system objects, namely calcium-, aluminium-rich inclusions (CAIs) from CV chondrites, have been used to define a 'canonical' value of $(^{26}Al/^{27}Al)_0$ (see review by MacPherson et al., 1995). Both *in situ* analyses of primitive, fine-grained CAIs (e.g.,

MacPherson, 2010) and bulk CAI measurements (Jacobsen et al., 2008; Larsen et al., 2011) yield $(^{26}Al/^{27}Al)_0 \sim 5.2\times10^{-5}$ and this value has been widely used as an appropriate starting value for the solar system as a whole. However, CAIs are both nucleosynthetically anomalous compared to bulk meteorites and have variable compositions (see review by Birck, 2004), so their reliability as a reference $(^{26}Al/^{27}Al)_0$ for the SPD as a whole is open to debate.

Improvements in bulk analytical techniques over the past decades (Galy et al., 2000; Bizzarro et al., 2004; Bizzarro et al., 2011) now allows differences of a few parts per million (ppm) in mass-independent Mg isotopic compositions, $\Delta'^{26}Mg_{DSM\text{-}3}$ (see definition in section 2.2), to be distinguished. This capability provides a valuable perspective on possible $(^{26}Al/^{27}Al)_0$ heterogeneity in solar system bodies. Schiller et al. (2010) and Kita et al. (2013) showed that the $\Delta'^{26}Mg_{DSM\text{-}3}$ of bulk chondrites correlate with their Al/Mg, suggesting a common, canonical $(^{26}Al/^{27}Al)_0$ in the parent bodies of these samples. On the other hand, Larsen et al. (2011) argued that the covariation of bulk chondrite $\Delta'^{26}Mg_{DSM\text{-}3}$ and $\varepsilon^{54}Cr$ (mass-independent variations in $^{54}Cr/^{52}Cr$) reflects variable contributions of a ^{54}Cr-rich component with high $(^{26}Al/^{27}Al)_0$, which, in general, was less abundant in bulk meteorites than in CAIs. In a third interpretation, Wasserburg et al. (2012) inferred nucleosynthetic Mg-isotope heterogeneity across the SPD, as is evident on a small scale by the different intercepts of Al-Mg isochrons of some unusual CAIs.

Thus, to date, the bulk chondrite $\Delta'^{26}Mg_{DSM\text{-}3}$ data have not clearly resolved the question of whether or not $(^{26}Al/^{27}Al)_0$ in the SPD was homogenous. Since the initial discussion outlined above, high-precision, bulk $\Delta'^{26}Mg_{DSM\text{-}3}$ measurements from further chondrite groups have been reported (van Kooten et al., 2016; Olsen et al., 2016; Larsen et al, 2016). Here we consider these additional data, together with new data of our own to reassess the problem. In particular, we have focused on better characterizing the composition of enstatite chondrites. As well as their bearing on the cause of bulk chondrite $\Delta'^{26}Mg_{DSM\text{-}3}$ variability, enstatite chondrites provide

a likely protolith composition for the Earth (e.g., Javoy et al., 1986). Comparison of the Al-Mg systematics of enstatite chondrites and Earth therefore provides a valuable means to determine the time at which the Earth, or its precursors, acquired elevated Al/Mg.

2 Methodology

2.1 Samples

We selected 18 chondrites for analysis (9 carbonaceous, 6 enstatite and 3 ordinary); samples were dominantly provided by the Natural History Museum London (Table 1). All except one meteorites are falls, which minimizes the chances of Al-Mg perturbation as a result of terrestrial weathering. As a major element, Mg isotope analyses do not require much material and we used bulk samples from 4 to 98 mg. Although the amount of material in the smaller samples was sufficient for precise Mg isotope measurements, whether or not they are representative of the whole meteorite is a consideration that we discuss below. We also compare the magnesium isotopic composition of Earth and Mars to these bulk chondrites. To this end, we analyzed a wide range of terrestrial rock standards (Table S2) and 4 martian samples (Table 1) comprising 3 shergottites and one nakhlite (3 antarctic finds supplied by NASA and one fall).

2.2 Notation

The δ^{x}Mg notation reports the relative deviation of the Mg isotope ratios ($^{25}Mg/^{24}Mg$ or $^{26}Mg/^{24}Mg$) from a reference isotopic composition (here the DSM-3 international, terrestrial standard):

$$\delta^{x}\mathrm{Mg}_{\text{DSM-3}} = \frac{\left(\frac{^{x}\mathrm{Mg}}{^{24}\mathrm{Mg}}\right)_{\text{sample}}}{\left(\frac{^{x}\mathrm{Mg}}{^{24}\mathrm{Mg}}\right)_{\text{DSM-3}}} - 1, \text{ where } x \text{ stands for 25 or 26.} \quad (1)$$

Following the IUPAC recommendation (see Coplen, 2011), we exclude the multiplier of 1000 traditionally used in this notation. Values of delta can then be expressed as fractions, ‰, ppm or otherwise, according to preference.

We express mass-independent anomalies in ^{26}Mg (i.e. the ^{26}Mg excesses or deficits relative to a given mass fractionation law) in terms of linearized expressions of delta in the Δ' notation (see Young and Galy, 2004 for discussion of the rationale of this approach):

$$\Delta'^{26}\mathrm{Mg}_{\text{DSM-3}} = \delta^{26}\mathrm{Mg}_{\text{DSM-3}} - \delta^{25}\mathrm{Mg}_{\text{DSM-3}} / \beta \quad (2)$$

where

$$\delta^{26}\mathrm{Mg}_{\text{DSM-3}} = \ln(\delta^{26}\mathrm{Mg}_{\text{DSM-3}} + 1) \text{ and } \delta^{25}\mathrm{Mg}_{\text{DSM-3}} = \ln(\delta^{25}\mathrm{Mg}_{\text{DSM-3}} + 1) \quad (3)$$

We use $\beta = 0.511$ which corresponds to a kinetic mass fractionation law (see Supplementary Materials for discussion of this value). Values of $\Delta'^{26}\mathrm{Mg}_{\text{DSM-3}}$ very closely approximate to the values for the more commonly used expressions of Δ^{26}Mg and δ^{26}Mg*. Subsequently in the text, we will abbreviate $\Delta'^{26}\mathrm{Mg}_{\text{DSM-3}}$, $\delta^{25}\mathrm{Mg}_{\text{DSM-3}}$ and $\delta^{26}\mathrm{Mg}_{\text{DSM-3}}$ to Δ'^{26}Mg, δ^{25}Mg, and δ^{26}Mg respectively.

2.3 Mg isotope measurements by MC-ICPMS

Details of sample digestion and chromatographic separation of Mg from the matrix are given in Supplementary Materials.

Our analytical protocol is documented in detail below but the key points can be summarized as follows. Given the small anticipated Δ'^{26}Mg differences, we measure intense Mg beams (> 2 nA on mass 24) over suitable durations (> 150 min) to obtain Δ'^{26}Mg precisions

of 2-3 ppm (2se). This consumes less than 40 μg Mg per sample. It is critical to assess influences on the accuracy of such measurements and, to this end, we have checked that our analytical uncertainties are in line with those expected from counting statistics and Johnson noise. We have also checked that our measured peaks are flat to high precision, and not impacted by interferences or ion-optical effects, and the results of these tests are described in Supplementary Materials.

Generalities

Mg isotope ratios were measured using a Thermo Finnigan Neptune MC-ICPMS, at the University of Bristol (Serial No. 1002). Samples were introduced using an ESI PFA MicroFlow nebulizer and an Apex Q introduction system, with an uptake rate of ~ 40 μL/min. Isotopes ^{24}Mg, ^{25}Mg and ^{26}Mg were collected simultaneously in three Faraday cups (L4, C and H4, respectively), using the 'medium' resolution entrance slit ($M/\Delta M$ 5-95% peak height ≥ ~ 5000). The Faraday cup amplifiers were internally calibrated for baseline and gain at the beginning of each analytical session.

In this study we employed a large capacity, dry interface pump (~ 100 m^3/h side channel/molecular drag pump in place of our former ~ 30 m^3/h standard rotary pump) with a high-sensitivity 'Jet' sampler cone. Contrary to some prior studies reporting high precision Δ'^{26}Mg measurements (Bizzarro et al., 2011; Schiller et al., 2015), we use an 'H' skimmer cone (see Table S1 for comparison with other studies' instrumental settings). The combination of Jet sampler and H skimmer cones yields a comparable sensitivity to that of standard sampler and X skimmer cones but lower sensitivity than Jet sampler plus X skimmer. The sensitivity we obtained is typically > 500 pA of $^{24}Mg^+$ for an Mg concentration of 1 μg/g using Jet sampler

and H skimmer cones. The H skimmer cones give sessions with more stable mass bias than X skimmer cones and lower molecular interferences such as CN and hydrides.

The standard-sample-standard bracketing procedure we used, with the DSM-3 international standard, yields both mass dependent isotopic data (via Eq. 1) and mass independent data (via Eq. 2 and 3). Sample Mg concentrations were adjusted to be within 5% of the DSM-3 Mg concentration (~ 4 μg/g), and drift in instrumental mass bias in the isotope ratios of samples is corrected using the mean of the isotope ratios of the bracketing DSM-3 analyses. A measurement sequence typically consisted of analyses of DSM-3 and sample, repeating until all samples (and duplicates) are measured, followed by a final DSM-3 analysis. A single analysis was comprised of 24 cycles of 8.389 s integration (i.e. a total data acquisition time of ~ 200 s). Prior to every analysis, the introduction system is rinsed by taking up 0.3M HNO_3 for 150 s followed by a 30 s on-peak blank measurement using a separate vial of 0.3M HNO_3. The mean on-peak intensities measured in the blanks for the entire sequence were subtracted from the intensities of the measured samples and from DSM-3 prior to calculating the intensity ratios. The $^{24}Mg^{+}$ on-peak blank intensity was ~ 0.05 pA, and rather constant over the ~ 20 h sequence, with the other Mg isotope blank intensities approximately in accordance with their isotopic abundances. The sample (and DSM-3) $^{24}Mg^{+}$ beam intensity was typically 2 nA.

Precision

To allow measurement of the intense Mg^{+} ion beams needed for high precision $\Delta'^{26}Mg$ determinations, the Faraday cup used to collect ^{24}Mg was connected to an amplifier with a 10^{10} Ω feedback resistor. This permits measurements of up to 3.2 nA without needing 10^{10} Ω

resistors on the amplifier circuits for the less abundant isotopes. However, to allow a comfortable margin for any intensity drift we typically measured ^{24}Mg beams ~ 2 nA.

Figure 1 shows typical precisions of Δ'^{26}Mg we obtain for our measurement procedure compared to a theoretical uncertainty model that considers the effects of counting statistics and Johnson-Nyquist noise on the precision (see Supplementary Materials for details on the uncertainty model). This uncertainty model gives a total uncertainty on Δ'^{26}Mg of 2.3 ppm to 1.4 ppm (2se) for a sample run according to our measurement routine (typically 2 nA on mass 24) repeated 20 to 50 times (Fig. 1). This is very close to the uncertainties reported in Table 1. Observed uncertainties are inevitably higher than the theoretical uncertainty due to additional sources of uncertainty in measuring samples. One possible contributor is rapid fluctuations in the plasma conditions, leading to a short-timescale variability in the instrumental fractionation (Andrén et al., 2004).

Terrestrial Standards

Terrestrial rock standards give mass-dependent Mg isotope ratios consistent with consensus literature values on these materials (see Fig. S4). For example, we obtained δ^{25}Mg = −0.114 ± 0.079 ‰ (2sd, n=6) for BIR-1 and δ^{25}Mg = −0.107 ± 0.042 ‰ (2sd, n=8) for BHVO-2. A point that needs to be highlighted is that these reproducibilities indicate that the high precisions apparent for individual analyses within a sequence (typically 0.01 ‰ and 0.02 ‰ (2se) for δ^{25}Mg and δ^{26}Mg, respectively) do not reflect the uncertainty on δ^{25}Mg values from one session to another (and sometimes even from one sequence to another within a single session) using the sample-standard bracketing technique. For instance, we measured the Cambridge solution standard to monitor such variability and its mean δ^{25}Mg in a sequence can vary from ~ −1.29 ± 0.02 ‰ to −1.40 ± 0.02 ‰ (2sd) depending on the analytical session,

although it was typically −1.34 ‰. Comparable variability is also evident in the literature; Figure S4 shows that different groups obtain quite a wide range of results for the same standards, demonstrating the challenge of obtaining accuracy of the same order as the precision using a bracketing technique for mass-dependent Mg isotope ratio measurements.

Such problems led some of us to develop a critical mixture double spiking approach for mass-dependent Mg isotopic analyses (Coath et al., 2017). This improves the reproducibility but average δ^{25}Mg values are quite consistent for samples run here by sample-standard bracketing and by Hin et al. (2017) using double spiking. In our experience, the relative difference in δ^{25}Mg between samples remain consistent from one session to another, and most importantly both δ^{26}Mg and δ^{25}Mg are shifted in a way that does not affect Δ'^{26}Mg. Thus, running samples at high intensity does not improve mass-dependent determinations, as might be anticipated at first glance from internal precision, but nonetheless produces data comparable to that obtained by other sample-standard bracketing approaches.

Our use of high intensity Mg^+ beams significantly improves the precision on Δ'^{26}Mg compared to most previous studies, and we achieve a precision comparable to that reported in Bizzarro et al. (2011) and subsequent papers from the StarPlan (Copenhagen) group (Larsen et al., 2011; Schiller et al., 2015; van Kooten et al., 2016; Olsen et al., 2016). For our terrestrial rock standards we obtain the following values of Δ'^{26}Mg: −2.4 ± 3.6 ppm (2se, n=8) for BHVO-2, 1.9 ± 2.3 ppm (2se, n=6) for BIR-1, 1.0 ± 1.7 ppm (2se, n=63) for JP-1 and 1.0 ± 2.0 ppm (2se, n=20) for San Carlos peridotite olivine (Fig. 2). Combining all the measurements on rock standards gives a terrestrial Δ'^{26}Mg of 0.8 ± 2.8 ppm (2se, n=97). This is consistent with previously reported high precision Δ'^{26}Mg values (Fig. 2), with mean Δ'^{26}Mg = −0.4 ± 1.0 ppm for DTS-2b, J12, BHVO-2 and BIR-2 in Bizzarro et al. (2011) and 0.4 ± 1.7 ppm for BHVO-2 and DTS-2b in Olsen et al. (2016), for example.

2.4 Al/Mg ratio measurements by MC-ICPMS

In this study, Al/Mg ratios were measured using a bracketing technique, on a Thermo Finnigan Neptune MC-ICPMS, at the University of Bristol (Serial No. 1020). Such simultaneous, Faraday cup measurements are similar to those made in some other Al-Mg studies of bulk meteoritic materials (e.g., Bizzarro et al., 2004, Jacobsen et al., 2008), which improve the precision of Al-Mg determination relative to traditional methods of peak jumping collection on a secondary electron multiplier. Samples were introduced using an ESI PFA MicroFlow nebulizer with an uptake rate of ~ 50 μL/min. A first attempt using a 'dry plasma' (with an ESI Apex HF desolvating system) associated with a 'Jet' sampler cone resulted in measured $^{27}Al/^{24}Mg$ which were not reproducible to within better than 3-4% between different sessions, despite the relative differences between chondrites being consistent from one session to another. We attributed this bias to a matrix effect and decided to use a 'wet plasma' mode (with a stable introduction system, SIS) and standard sampler and skimmer cones, less subject to matrix effects. With this setup, the reproducibility for the measured atomic $^{27}Al/^{24}Mg$ of individual chondrites is typically improved to better than 1% (2sd), based on 8 repeats of individual sample run in two separate sessions.

We measured ^{24}Mg and ^{27}Al isotopes simultaneously on Faraday cups (on L4 and H4, respectively). Two reference solutions (both in 0.3M HNO_3) were prepared from 10 μg/g solutions of pure Mg and Al standards (dilutions of SCP Science *Plasma*CAL Mg 1000 μg/g and Al 1000 μg/g standards in 4% HNO_3, respectively): one with an atomic $^{27}Al/^{24}Mg$ of 1.8546 close to BHVO-2 and the other closer to chondrites, $^{27}Al/^{24}Mg = 0.1005$. Our reported values of $^{27}Al/^{24}Mg$ assume the quoted concentrations on the purchased solutions are accurate, which is not necessarily secure at a one percent level, but we further calibrate against well characterized reference materials (see below). Aliquots of standards and samples prior to Mg

separation chemistry were prepared to give solutions of ~ 1.5 μg/g Mg in 0.3M HNO_3. Sample and standard ^{24}Mg intensities were closely matched, typically within 5%. Sample measurements were bracketed with the appropriate reference solution for basaltic or chondritic composition, respectively. Measurements were made using the 'medium' resolution entrance slit.

A single measurement consisted of 20 cycles of 8.389 s integration time (i.e. a total data acquisition time of ~ 168 s), with a wash time between samples of 100 s. The $^{27}Al/^{24}Mg$ reported in Table 1 are atomic ratios calculated as the blank corrected measured $^{27}Al/^{24}Mg$ of the sample over the mean, blank-corrected measured $^{27}Al/^{24}Mg$ of the bracketing reference solution, multiplied by the atomic $^{27}Al/^{24}Mg$ of the reference solution. Correcting for the instrumental blank, measured in a 0.3M HNO_3 solution, does not change the $^{27}Al/^{24}Mg$ beyond measurement uncertainty, as the blank signal is low (typically of 0.04 pA on ^{24}Mg and 0.01 pA on ^{27}Al) compared to the signals of standards and samples (typically 25 pA on ^{24}Mg and 3 pA on ^{27}Al).

An atomic $^{27}Al/^{24}Mg$ of 1.8792 ± 0.0078 (2sd, n=12) is obtained for BHVO-2, which is consistent with the value of 1.873 ± 0.073 (2sd) recommended by the United States Geological Survey (USGS) and within ~ 0.5% of the value of 1.8712 ± 0.0027 (2sd, n=9) reported for BHVO-2 by Paton et al. (2012). We also measured BCR-2 which gave an atomic $^{27}Al/^{24}Mg$ of 3.7387 ± 0.0130 (2sd, n=12), which is also within ~ 0.5% of the value of 3.747 ± 0.035 (2se, n=20) reported for this basalt by Jacobsen et al. (2008) and the recommended USGS value of 3.764. Our mean $^{27}Al/^{24}Mg$ measured for two CI chondrites is 0.1017 ± 0.0016 (2sd, n=16), Table 1. This agrees well with the established, literature CI compilation value of 0.1012 ± 0.0029 (2sd) (Lodders, 2003) and the mean of 0.0998 ± 0.0056 (2sd) for high precision measurements of three CI meteorites by Larsen et al. (2011). The latter used the same methodology documented in Paton et al. (2012), who reported a lower $^{27}Al/^{24}Mg$ = 0.09781 ±

0.00029 for a 2.5 g dissolution of Ivuna (CI chondrite). The authors suggested that the minor difference relative to the Larsen et al. (2011) data likely reflected sample heterogeneity in the different ~ 20 mg sample dissolutions of the Larsen et al. (2011) study. Similar arguments might apply to the comparison between the Paton et al. (2012) $^{27}Al/^{24}Mg$ for Ivuna and our CI data, given our good agreement for BHVO-2.

3 Results

Our new Mg isotopic measurements show small variations between bulk chondrites, with $\Delta'^{26}Mg$ from −5.5 ± 1.6 ppm to +22.0 ± 3.0 ppm (Table 1), comparable to the range in previous high precision studies (Schiller et al., 2010; Larsen et al., 2011, 2016; van Kooten et al., 2016). Carbonaceous chondrites, excluding CR chondrites, are characterized by higher $\Delta'^{26}Mg$ values than ordinary and enstatite chondrites. By making measurements of Orgueil, bracketed against ordinary chondrites instead of the standard DSM-3, we have better resolved the difference in $\Delta'^{26}Mg$ between CI and ordinary chondrites to be 6.9 ± 1.7 ppm (2se, n=60, Table S5), within uncertainty of the difference of 8.6 ± 1.4 ppm reported by Larsen et al. (2011).

Significantly, there is a correlation between $\Delta'^{26}Mg$ and $^{27}Al/^{24}Mg$ for all chondrites, other than the CR group, both in data of our own and from other high precision studies (Schiller et al., 2010; Larsen et al., 2011, 2016; van Kooten et al., 2016), see Figure 3a and Table 2. Our magnesium isotope analyses for bulk enstatite chondrites expand the existing dataset of single values reported by Larsen et al. (2011) and Schiller et al. (2010). Our new measurements show covariations in $\Delta'^{26}Mg$ and $^{27}Al/^{24}Mg$, with similar slope, albeit with large uncertainty, to that for all other bulk chondrites except CRs, but offset to slightly higher $\Delta'^{26}Mg$ (Fig. 3a, Table 2). To further assess this small difference in $\Delta'^{26}Mg$ between enstatite and ordinary chondrites, we

have measured the EL chondrite Khairpur bracketed against H ordinary chondrites (Zag and Ceniceros), the group with most similar Al/Mg to EL chondrites (Lodders and Fegley, 1998), and document a difference of 2.3 ± 1.8ppm (2se, n=51, Table S6).

We show estimated compositions of the Earth and Mars in Fig. 3b, using bulk planetary $^{27}Al/^{24}Mg$ values from Palme and O'Neill (2003) and Sanloup et al. (1999) respectively, in conjunction with our mean $\Delta'^{26}Mg$ for terrestrial (Table S2) and martian (Table 1) samples. Both of these planetary compositions plot to the right of all bulk meteorite compositions, with the Earth having higher $\Delta'^{26}Mg$ than Mars (Fig. 3b).

4 Discussion

4.1 The canonical isochron

In interpreting the significance of the correlation of $\Delta'^{26}Mg$ with Al/Mg (Fig. 3a), it is first important to discuss the origin of Al/Mg variability between bulk chondrites. Differences in the major element compositions of chondrite groups have long been related to nebular sorting of distinct precursor components. The influential conceptual model of Larimer and Anders (1970) argued for partial separation of refractory phases (enriched in Al) from main silicate minerals (containing the bulk of Mg) and metal, which condensed from the SPD over different temperature intervals. If bulk chondrite compositional contrasts in Al/Mg are set by sorting of these early-formed, nebular components, then associated variations in $\Delta'^{26}Mg$ are expected, with a highly radiogenic refractory component and an unradiogenic silicate component. In this context, an array of bulk chondrite analyses on an Al-Mg isochron diagram, such as Fig. 3a, should give a 'primordial' isochron with a slope yielding the $(^{26}Al/^{27}Al)_0$ at the time of

formation of these precursor phases. A single array would indicate homogeneous $(^{26}Al/^{27}Al)_0$ in the different precursor materials. To first order, this is what we observe (Fig. 3a).

The best fit slope and intercept of all high precision, bulk chondrite data, except enstatite chondrites and CR chondrites, yield $(^{26}Al/^{27}Al)_0$ of $(4.67 \pm 0.78)\times10^{-5}$ and $(\Delta'^{26}Mg)_0$ of -31.6 ± 5.7 ppm, respectively (Fig. 3a), calculated using the Isoplot v3 software on the 95% confidence interval (Ludwig, 2003). Note that 95% confidence intervals are calculated by multiplying the *a priori* uncertainties of the York regression by the square root of the MSWD and by the *t*-distribution critical value at 95% confidence. This calculated $(^{26}Al/^{27}Al)_0$ is within uncertainty of a canonical value of ~ 5.2×10^{-5}, as defined by bulk CAIs analyzed by Jacobsen et al. (2008) and Larsen et al. (2011). Kita et al. (2013) previously interpreted literature bulk chondrite data in a similar fashion, and we believe that new data of our own and others strengthen this point of view.

Along similar lines, Schiller et al. (2010) argued that their correlation between $\Delta'^{26}Mg$ and Al/Mg in bulk carbonaceous chondrites represented mixing with CAIs. An equivalent trend is evident in our work (Fig. 3a) but a key difference is the relationship of ordinary and carbonaceous chondrites. Schiller et al. (2010) specifically noted that ordinary chondrites, with lower Al/Mg, did not have $\Delta'^{26}Mg$ significantly lower than non CAI-bearing carbonaceous chondrites. In contrast, we find that a line through bulk carbonaceous chondrite (excluding CRs) data and CAIs back projects through our ordinary chondrite compositions (Fig. 3b). This is in keeping with the analyses of Larsen et al. (2011), and admittedly is difficult to resolve in the Schiller et al. (2010) data due to their lower precision. The most straight-forward interpretation of the observation that bulk ordinary chondrites, bulk carbonaceous chondrites (excluding CRs) and CAIs are all co-linear in Fig. 3 and 4 is that they had the same $(^{26}Al/^{27}Al)_0$ and $(\Delta'^{26}Mg)_0$. If this inference is correct, it validates the use of Al-Mg dating amongst these diverse objects.

Our implied suggestion of primordial Al/Mg differences between bulk chondrites might seem at odds with ~ 2-4 Ma younger Al-Mg ages for chondrules (see recent review by Nagashima et al., 2018), the chief constituents of many chondrites. Yet, Larimer and Anders (1970) noted that the formation of chondrules does not seem to be related to the fractionations that set the bulk compositions of the different chondrite groups. Consequently, Larimer and Anders (1970) argued that chondrules formed after the nebular processes that determined the major element contrasts between bulk chondrites. Thus, chondrules represent reprocessed material from a reservoir whose composition had already been set by differential sorting of precursor phases. These ideas are entirely in keeping with our interpretations of the Al-Mg systematics. We illustrate that most bulk chondrite groups plot on an array colinear with the canonical CAI slope (Fig. 3 and 4), reflecting compositions set by different mixtures of early-formed precursors. An analogous argument was made for the Mn-Cr system by Trinquier et al. (2008). We interpret the range of younger Al-Mg *internal* isochron ages in chondrules to reflect various generations of (re-)melting events (e.g., Nagashima et al., 2018), which reset the Al-Mg systematics at a chondrule length scale but not at the scale of bulk chondrites.

Bulk chondrite compositions with high Al/Mg were attributed to preferential incorporation of a refractory phase in the model of Larimer and Anders (1970). This process is well illustrated with the effect of CAI addition to a CI composition (Fig. 4a), although other refractory phases might also contribute (e.g., some of the hibonites plotted in Fig. 4b would also be appropriate refractory components). As well as primary differences in proportions of CAIs incorporated into different meteorite parent bodies, unrepresentative sampling of the bulk meteorites by relatively small sample aliquots can also influence analyses. We concur with Schiller et al. (2010) that the former process is likely the dominant control on the variability in Al/Mg and corresponding Δ'^{26}Mg among carbonaceous chondrites, but the latter creates additional variability along the same trajectory. Representative sampling is most problematic

for CV chondrites (see Hezel et al., 2008), where chance inclusion or exclusion of macroscopic CAIs can significantly bias the measured composition (e.g., Stracke et al., 2012). For instance, our sample of Allende has Δ'^{26}Mg of 22.0 ± 3.0 ppm and ^{27}Al/^{24}Mg of 0.1689 ± 0.0004, which compares to two pieces of Allende analyzed in Schiller et al. (2010) that have Δ'^{26}Mg of 20.2 ± 6.0 and 11.7 ± 6.0 ppm with ^{27}Al/^{24}Mg of 0.131 ± 0.003 and 0.124 ± 0.003, respectively.

Evidently, addition of minor amounts of an early-formed refractory phase, such as CAIs, to a CI composition can generate the range of Δ'^{26}Mg in carbonaceous chondrites (Fig. 4a). Larimer and Anders (1970) further argued that ordinary and enstatite chondrites were missing increasing amounts of the refractory component present in CIs, and this would duly account for their lower Al/Mg and Δ'^{26}Mg. Namely, these bulk compositions are more dominated by the unradiogenic silicate component.

Although a canonical slope describes most of the variability of the data in Fig. 3, there is evident scatter. While only a subtle offset, the enstatite chondrites all have systematically higher Δ'^{26}Mg than the main array. They apparently define a slightly shallower slope with an initial ^{26}Al/^{27}Al abundance of $(3.75 \pm 2.09)\times10^{-5}$ and an initial Δ'^{26}Mg of −22.7 ± 13.0 ppm (Table 2), although their small spread in Al/Mg makes it rather poorly constrained. We suggest that the array dominantly reflects a difference between EL and EH chondrite groups. The EH chondrites have higher Al/Mg than the EL chondrites (see Lodders and Fegley, 1998), which will be associated with higher Δ'^{26}Mg if this difference was created early, as we argue above for the other chondrite groups. In detail, there is some overlap of Al/Mg between our samples from EL and EH groups (Table 1), but this likely reflects Al/Mg heterogeneity within our relatively small samples. As we show for ordinary chondrites (see Supplementary Materials), there is no Δ'^{26}Mg variation associated with hand specimen scale Al/Mg variability and we would expect the same to be the case for the enstatite chondrites. We suggest that the ostensibly

systematic covariations of Al/Mg with Δ'^{26}Mg for individual enstatite chondrite samples in Fig 3a is chance, even if the overall slope of the array defined by EH and EL variability is significant (Table 2).

While the elevated Δ'^{26}Mg of the enstatite chondrites might simply reflect mass independent isotopic variability within their nebula source region, in no other isotopic systems are the enstatite chondrites anomalous with respect to a common composition for ordinary and carbonaceous chondrites (e.g., Dauphas, 2017). This suggests that the distinctive Δ'^{26}Mg of enstatite chondrites may reflect timing and radiogenic ingrowth, rather than nucleosynthetic inheritance. In this context, it is pertinent that the low Mg/Si of enstatite chondrites is typically attributed to significant loss of the most refractory phases, including a fraction of forsterite condensates (Larimer and Anders, 1970; Hutson and Ruzicka, 2000). If the highly reduced conditions necessary for formation of enstatite chondrites are a result of an environment with C/O higher than solar values, as commonly proposed (e.g., Larimer and Bartholomay, 1979), this decreases by several hundred degrees the temperature at which major silicate phases condense compared to nebular conditions inferred to be associated with formation of ordinary and carbonaceous chondrites. We speculate that the relatively low temperature required for condensation of precursor olivine in a reduced environment delays the time at which it can be removed to form the enstatite chondrite reservoir. Moreover, the commonly invoked formation setting of enstatite chondrites close to the Sun will result in a slow cooling rate and further delays the formation of the enstatite chondrite reservoir compared to the other chondrite groups.

A detailed assessment of the timescale of enstatite chondrite formation is beyond the scope of this contribution but will depend on poorly constrained parameters such as ambient C/O, degree of re-equilibration and the rate of nebula cooling during condensation. Simplistically, the Δ'^{26}Mg of a solar composition evolves from an initial value of −34 ppm to the best-fit intercept of the enstatite chondrite array at −22 ppm in ~ 500 ka. This value provides

a sense of the inferred delay in enstatite chondrite reservoir formation relative to carbonaceous and ordinary chondrites, but clearly more work is required both to better define isotopic differences and model the results.

The CR chondrites show a more marked departure from the array with canonical slope than the enstatite chondrites and a greater range in compositions (Fig. 3a). We propose that some of this variability may be secondary. Two CR finds from van Kooten et al. (2016) plot to very high Al/Mg, suggestive of possible Mg loss from terrestrial weathering (e.g., Grossman and Score, 1996) for these desert finds. This creates an impression of an isochron with zero slope for the CR chondrites as a whole, which we interpret as modern perturbation of Al/Mg, long after ^{26}Al was extant. However, all except one high-precision CR measurements have lower Δ'^{26}Mg than other carbonaceous chondrites at comparable Al/Mg to CIs. More generally, the low Δ'^{26}Mg of various components of metal-rich carbonaceous chondrites have been argued to reflect primordial ^{26}Al-poor molecular cloud material in the accretion region of these meteorites (van Kooten et al., 2016; Olsen et al., 2016). However, this hypothesis is challenged by recent studies reporting a Hf-W age for CR chondrites of 3.6 ± 0.6 Ma after CAI formation based on analyses of metal and chondrule fractions, magnetic separates and bulk chondrite samples (Budde et al., 2018), in agreement with the mean Al-Mg age for CR chondrules of 3.7 ± 0.3 Ma (Schrader et al., 2017). The fact that these two different short-lived chronometers give consistent ages for the formation of CR chondrules is in keeping with ^{26}Al/^{27}Al at the canonical level in the formation region of CR chondrules.

Not only are CR chondrites anomalous in terms of their Mg isotopic compositions but it is well established that they have characteristics distinct from other chondrite groups. Most strikingly, they have extreme δ^{15}N (~ 140-190‰ for CRs compared to δ^{15}N < 100‰ for the other chondrites, e.g., review by Weisberg et al., 1995), which emphasises the particularity of this chondrite group compared to other carbonaceous chondrites. Therefore, low Δ'^{26}Mg of the

CR meteorites may be associated with the anomalous $\delta^{15}N$ and it is not necessarily indicative of low $(^{26}Al/^{27}Al)_0$.

We have thus far argued that $\Delta'^{26}Mg$ variations in bulk chondrites can be explained by differences in their Al/Mg and a near homogeneous, canonical $(^{26}Al/^{27}Al)_0$. An alternative interpretation of the $\Delta'^{26}Mg$ variability of bulk chondrites focused on a covariation between $\Delta'^{26}Mg$ and $\varepsilon^{54}Cr$ and invoked $(^{26}Al/^{27}Al)_0$ variability between chondrite parent bodies (Larsen et al., 2011, later re-emphasized by van Kooten et al. 2016). With the additional high precision data on bulk chondrites since the original publication, there remains no clear correlation between $\Delta'^{26}Mg$ and $\varepsilon^{54}Cr$ (Fig. 5). The original $\Delta'^{26}Mg$ and $\varepsilon^{54}Cr$ correlation of Larsen et al. (2011) was essentially defined by the ordinary chondrites and CI chondrites. As highlighted above, however, the difference in $\Delta'^{26}Mg$ between these two groups is well explained by differences in their Al/Mg and a uniform, canonical $(^{26}Al/^{27}Al)_0$. Thus, the original, widely cited evidence for $(^{26}Al/^{27}Al)_0$ heterogeneity can be readily interpreted in an opposite sense.

Whilst we argue that largely homogeneous, canonical $(^{26}Al/^{27}Al)_0$ is the most straightforward way to interpret the observations discussed above, there is apparently conflict with the findings of Schiller et al. (2015). These authors infer a factor of 4 variability of $(^{26}Al/^{27}Al)_0$ in the SPD, reporting $(^{26}Al/^{27}Al)_0$ of ~ 1.3×10^{-5} for the angrite parent body, as determined from internal Al-Mg isochrons pinned to Pb-Pb ages of angrite meteorites. However, using angrites as a time anchor for ^{26}Al-^{26}Mg is questionable given the likely disturbance of the plagioclase phase in these meteorites (e.g., Sanborn et al., 2015; Baker et al., 2005). In contrast, Sanborn et al. (2019) recently reported coherent ages for ^{26}Al-^{26}Mg and ^{53}Mn-^{53}Cr in two carbonaceous achondrites NWA 6704 and NWA 6693, which are also consistent with their absolute U-isotope corrected ^{207}Pb-^{206}Pb age (Amelin et al., 2019). The authors took care of carefully demonstrating the suitability of these two achondrites as time

anchors for short-lived chronometers. Our work provides independent evidence for the homogeneity of $^{26}Al/^{27}Al$ in the solar system which must underpin such consistency.

4.2 Position of planetary bodies relative to the canonical isochron

The estimated bulk composition of the Earth lies to the right of our chondritic isochron (Fig. 3b). Thus the Earth cannot be made from unmodified bulk chondritic materials. Indeed, from its non-chondritic mass-dependent Mg isotope composition (Hin et al., 2017), the elevated Al/Mg of the Earth has been argued to result from preferential loss of Mg (and more volatile elements) during collisional accretion. Similar arguments have been proposed from Si isotopic measurements (Pringle et al., 2014). Given continued support of enstatite chondrite-like building blocks for the Earth (e.g., Javoy et al., 1986; Dauphas, 2017), at least in terms of their isotopic compositions (^{17}O, ^{48}Ca, ^{50}Ti, ^{54}Cr, ^{64}Ni, ^{92}Mo, ^{100}Ru), the difference in $\Delta'^{26}Mg$ between Earth and enstatite chondrites can be used to constrain the timing of the Earth's increase in Al/Mg. As can be seen in Fig. 3b, the $\Delta'^{26}Mg$ of the Earth is similar to the mean value of the enstatite chondrites, requiring that the Earth acquired its high Al/Mg after most of the ^{26}Al had decayed. Critically, this observation highlights that the high terrestrial Al/Mg is not an inherited, nebula feature but was acquired relatively late during accretion.

We can explore this concept a little more quantitatively. The variability of our enstatite chondrite analyses complicates the choice of a terrestrial protolith composition. We use a mean $^{27}Al/^{24}Mg$ of 0.085 for enstatite chondrites from Lodders and Fegley (1998) and use this with the regression through our enstatite chondrite analyses to derive a representative $\Delta'^{26}Mg \sim 0 \pm 2$ ppm at this $^{27}Al/^{24}Mg$. Figure 6 illustrates how early an instantaneous Al/Mg fractionation from an enstatite chondrite composition with canonical $(^{26}Al/^{27}Al)_0$ can occur without

generating an Earth with too high Δ'^{26}Mg. As can be seen, several half-lives of ^{26}Al decay are required before terrestrial protoliths can have acquired their high Al/Mg. Vapour loss may have initiated earlier in a more realistic scenario where the change in Al/Mg was not instantaneous. Our measurements nonetheless suggest that Al/Mg fractionation occurs after much of the ^{26}Al has decayed. Thus the process of vapour loss, that drives Al/Mg fractionation, is unlikely to be driven by heating from the decay of ^{26}Al alone (Young et al., 2019) but requires an additional energy source, as might occur from impacts of larger planetesimals (Hin et al, 2017).

Models of collision-driven vapour loss of Mg (and Si) are most effective in small bodies with weak gravity fields but require sufficiently large bodies to deliver enough energy to drive melting and subsequent evaporation. As a result of these trade-offs, the process is optimal for bodies ~ 1000 km in radius (Hin et al., 2017). Therefore, our Mg isotope data suggest that such bodies are formed > 1.5 Ma post CAIs. Our upper bound on the rate of planetesimal accretion inferred from vapour loss is a useful complement to the rapid timescales of growth determined for planetesimal core formation (~ 0.1 to 0.3 Ma after CAIs), from W isotopic measurements of iron meteorites (e.g., Kruijer et al., 2014). The latter records the process of iron segregation, which may dominantly reflect events occurring on smaller bodies at the onset of melting, whereas our estimate is sensitive to vapour loss in later collisions. We can note that our estimate is in line with the rapid timescales for volatile loss determined from Mn-Cr (within 2 Ma post CAIs; e.g., Trinquier et al., 2008) and Rb-Sr (within ~ 1 Ma post CAIs; e.g., Hans et al., 2013) systematics.

A similar exercise can be undertaken for Mars. Our analyses of martian meteorites, which we take to be representative of martian mantle, have significantly lower Δ'^{26}Mg than the Earth (Fig. 3b). Indeed, the martian samples have some of the lowest Δ'^{26}Mg in our study but overlap with values for ordinary chondrites and enstatite chondrites. Sanloup et al. (1999)

showed that a mixture of 55% ordinary chondrites (H) and 45% enstatite chondrites (EH) reproduces the oxygen isotopic composition of Mars. There is little scope for any preferential ingrowth of ^{26}Mg during the evolution of Mars given its low Δ'^{26}Mg, as noted for the Earth. Sadly, geochemical estimates of Mars' bulk Al/Mg rely on models that select a single chondrite class (for instance, CI chondrites in e.g., Wänke and Dreibus, 1988) or a mixture of various chondrite classes (for instance, ordinary and enstatite chondrites in e.g., Sanloup et al., 1999; Brasser et al., 2017) to represent the bulk composition of Mars. Because its Al/Mg is so poorly constrained, it is difficult to make a more quantitative estimate of the timing of a putative change in its Al/Mg.

5 Conclusion

With the exception of CRs and enstatite chondrites, the suite of bulk chondrites (CV, CI, CM, CO and CK carbonaceous chondrites, H and LL ordinary chondrites) define a primordial Al-Mg isochron. The slope of this array yields $(^{26}Al/^{27}Al)_0 \sim (4.7\pm0.8)\times10^{-5}$ within uncertainty of the canonical value previously defined by CAIs (Jacobsen et al. 2008; Larsen et al. 2011). The sample array in the isochron diagram is indicative of a near homogenous initial $(^{26}Al/^{27}Al)_0$ during formation of CAIs and precursor grains to the different meteorite groups. This interpretation supports the use of the Al-Mg systematics as a short-lived chronometer. We argue that enstatite chondrites have slightly higher Δ'^{26}Mg due to relatively late condensation and loss of refractory phases, including a fraction of forsterite condensates. Regarding CR chondrites, we argue that their anomalously low $(\Delta'^{26}Mg)_0$ is possibly related to their markedly elevated δ^{15}N.

Mars and the Earth plot to the right of the chondritic isochron, with the Earth being more radiogenic than Mars. This indicates that these two planetary bodies cannot be made from unmodified bulk chondritic materials but instead experienced Al/Mg fractionation, for instance due to Mg loss during collisional accretion (Hin et al., 2017). A simple model of instantaneous fractionation requires that such Al/Mg fractionation process on the planetesimal protoliths of these planets must have occurred after several half-lives of ^{26}Al decay (> 1.5 Ma post CAIs). This provides a useful, independent constraint on the initial timescale of accretional growth of the Earth.

Acknowledgements

This work was supported by a grant from the European Research Council (ERC Adv grant 321209 — ISONEB).

References

Amelin, Y., Koefoed, P., Iizuka, T., Fernandes, V.A., Huyskens, M., Yin, Q.-Z., Irving, A.J., 2019. U-Pb, Rb-Sr and Ar-Ar systematics of the ungrouped achondrites Northwest Africa 6704 and Northwest Africa 6693. Geochim. Cosmochim. Acta 245, 628-642.

Andrén, H., Rodushkin, I., Stenberg, A., Malinovsky, D., Baxter, D.C., 2004. Sources of mass bias and isotope ratio variation in multi-collector ICP-MS: optimization of instrumental parameters based on experimental observations. J. Anal. At. Spectrom. 19, 1217-1224.

Baker, J., Bizzarro, M., Wittig, N., Connelly, J., Haack, H., 2005. Early planetesimal melting from an age of 4.5662 Gyr for differentiated meteorites. Nature 436, 1127-1131.

Birck, J.-L., 2004. An overview of isotopic anomalies in extraterrestrial materials and their nucleosynthetic heritage. Rev. Min. Geochem. 55, 25-64.

Bizzarro, M., Baker, J.A., Haack, H., 2004. Mg isotope evidence for contemporaneous formation of chondrules and refractory inclusions. Nature 431, 275-278.

Bizzarro, M., Paton, C., Larsen, K., Schiller, M., Trinquier, A., Ulfbeck, D., 2011. High-precision Mg-isotope measurements of terrestrial and extraterrestrial material by HR-MC-ICPMS – implications for the relative and absolute Mg-isotope composition of the bulk silicate Earth. J. Anal. At. Spectrom. 26, 565-577.

Brasser, R., Mojzsis, S.J., Matsumura, S., Ida, S., 2017. The cool and distant formation of Mars. Earth Planet. Sci. Lett. 468, 85-93.

Budde, G., Kruijer, T.S., Kleine, T., 2018. Hf-W chronology of CR chondrites: Implications for the timescales of chondrule formation and the distribution of ^{26}Al in the solar nebula. Geochim. Cosmochim. Acta 222, 284-304.

Coath, C.D., Elliott, T., Hin, R.C., 2017. Double-spike inversion for three-isotope systems. Chem. Geol. 451, 78-89.

Coplen, T.B., 2011. Guidelines and recommended terms for expression of stable-isotope-ratio and gas-ratio measurement results. Rapid Commun. Mass Spectrom. 25, 2538-2560.

Dauphas, N., 2017. The isotopic nature of the Earth's accreting material through time. Nature 541, 521-524.

Galy, A., Young, E.D., Ash R.D., O'Nions R.K., 2000. The formation of chondrules at high gas pressures in the solar nebula. Science 290, 1751-1753.

Grossman, J.N., Score, R., 1996. Recently classified specimens in the United States Antarctic Meteorite Collection (1994-1996). Meteorit. Planet. Sci. 31, A161-A174.

Hans, U., Kleine, T., Bourdon, B., 2013. Rb-Sr chronology of volatile depletion in differentiated protoplanets: BABI, ADOR and ALL revisited. Earth Planet. Sci. Lett. 374, 204-214.

Hezel, D.C., Russell, S.S., Ross, A.J., Kearsley, A.T., 2008. Modal abundances of CAIs: Implications for bulk chondrite element abundances and fractionations. Meteorit. Planet. Sci. 43, 1879-1894.

Hin, R.C., Coath, C.D., Carter, P.J., Lai Y.J., Pogge von Strandmann, P.A.E., Willbold, M., Leinhardt, Z.M., Walter, M.J., Elliott, T., 2017. Mg isotope evidence that collisional vapour loss shapes planetary compositions. Nature 549, 511-515.

Hutson, M., Ruzicka, A., 2000. A multi-step model for the origin of E3 (enstatite) chondrites. Meteorit. Planet. Sci. 35, 601-608.

Jacobsen, B., Yin, Q.-Z., Moynier, F., Amelin, Y., Krot, A.N., Nagashima, K., Hutcheon, I.D., Palme, H., 2008. ^{26}Al-^{26}Mg and ^{207}Pb-^{206}Pb systematics of Allende CAIs: Canonical solar initial ^{26}Al/^{27}Al ratio reinstated. Earth Planet. Sci. Lett. 272, 353-364.

Javoy, M., Pineau, F., Delorme, H., 1986. Carbon and nitrogen isotopes in the mantle. Chem. Geol. 57, 41-62.

Kita, N.T., Yin, Q.-Z., MacPherson, G.J., Ushikubo, T., Jacobsen, B., Nagashima, K., Kurahashi, E., Krot, A.N., Jacobsen, S.B., 2013. ^{26}Al-^{26}Mg isotope systematics of the first solids in the early solar system. Meteorit. Planet. Sci. 48, 1383-1400.

Kruijer, T.S., Touboul, M., Fischer-Gödde, M., Bermingham, K.R., Walker, R.J., Kleine, T., 2014. Protracted core formation and rapid accretion of protoplanets. Science 344, 1150-1154.

Larimer, J.W., Anders, E., 1970. Chemical fractionation in meteorites – III. Major element fractionations in chondrites. Geochim. Cosmochim. Acta 34, 367-387.

Larimer, J.W., Bartholomay, M., 1979. The role of carbon and oxygen in cosmic gases: some applications to the chemistry and mineralogy of enstatite chondrites. Geochim. Cosmochim. Acta 43, 1455-1466.

Larsen, K.K., Trinquier, A., Paton, C., Schiller, M., Wielandt, D., Ivanova, M.A., Connelly, J.N., Nordlund, A., Krot, A.N., Bizzarro, M., 2011. Evidence for magnesium isotope heterogeneity in the solar protoplanetary disk. Astrophys. J. 735, L37-L43.

Larsen, K.K., Schiller, M., Bizzarro, M., 2016. Accretion timescales and style of asteroidal differentiation in an ^{26}Al-poor protoplanetary disk. Geochim. Cosmochim. Acta 176, 295-315.

Liu, M.-C., Chaussidon, M., Göpel, C., Lee, T., 2012. A heterogeneous solar nebula as sampled by CM hibonite grains. Earth Planet. Sci. Lett. 327-328, 75-83.

Lodders, K., 2003. Solar system abundances and condensation temperatures of the elements. Astrophys. J. 591, 1220-1247.

Lodders, K., Fegley, B. Jr., 1998. The Planetary Scientist's Companion. Oxford: Oxford University Press. 371 p.

Ludwig, K.R., 2003. Isoplot 3.00, a geochronological toolkit for Microsoft Excel (Berkeley Geochronology Center Special Publication No. 4, Berkeley, CA).

MacPherson, G.J., Davis, A.M., Zinner, E.K., 1995. The distribution of aluminium-26 in the early Solar System – A reappraisal. Meteoritics 30, 365-386.

MacPherson, G.J., Bullock, E.S., Janney, P.E., Kita, N.T., Ushikubo, T., Davis, A.M., Wadhwa, M., Krot, A.N., 2010. Early solar nebula condensates with canonical, not supracanonical, initial ^{26}Al/^{27}Al ratios. Astrophys. J. 711, L117-L121.

Nagashima, K., Kita, N.T., Luu, T.-H., 2018. ^{26}Al-^{26}Mg systematics of chondrules. In Chondrules: Records of Protoplanetary Disk Processes (eds. S.S. Russell, H.C. Connolly and A. Krot).

Olsen, M.B., Wielandt, D., Schiller, M., van Kooten, E.M.M.E., Bizzarro, M., 2016. Magnesium and ^{54}Cr isotope compositions of carbonaceous chondrite chondrules – Insights into early disk processes. Geochim. Cosmochim. Acta 191, 118-138.

Palme, H., O'Neill, H.S.C., 2003. Cosmochemical estimates of mantle composition. Treatise On Geochemistry, Vol. 2. Elsevier, New-York, pp. 1-39.

Paton, C., Schiller, M., Ulfbeck, D., Bizzarro, M., 2012. High-precision $^{27}Al/^{24}Mg$ ratio determination using a modified isotope-dilution approach. J. Anal. At. Spectrom. 27, 644-652.

Pringle, E.A., Moynier, F., Savage, P.S., Badro, J., Barrat, J.-A., 2014. Silicon isotopes in angrites and volatile loss in planetesimals. Proc. Natl. Acad. Sci. USA 111, 17029-17032.

Sanborn, M.E., Carlson, R.W., Wadhwa, M., 2015. $^{147,146}Sm$-$^{143,142}Nd$, ^{176}Lu-^{176}Hf, and ^{87}Rb-^{87}Sr systematics in the angrites: Implications for chronology and processes on the angrite parent body. Geochim. Cosmochim. Acta 171, 80-99.

Sanborn, M.E., Wimpenny, J., Williams, C.D., Yamakawa, A., Amelin, Y., Irving, A. J., Yin, Q.-Z., 2019. Carbonaceous achondrites Northwest Africa 6704/6693: Milestones for early Solar System chronology and genealogy. Geochim. Cosmochim. Acta 245, 577-596.

Sanloup, C., Jambon, A., Gillet, P., 1999. A simple chondritic model of Mars. Phys. Earth Planet. Inter. 112, 43-54.

Schiller, M., Handler, M.R., Baker, J.A., 2010. High-precision Mg isotopic systematics of bulk chondrites. Earth Planet. Sci. Lett. 297, 165-173.

Schiller, M., Connelly, J.N., Glad, A.C., Mikouchi, T., Bizzarro, M., 2015. Early accretion of protoplanets inferred from a reduced inner solar system ^{26}Al inventory. Earth Planet. Sci. Lett. 420, 45-54.

Schrader, D.L., Nagashima, K., Krot, A.N., Ogliore, R.C., Yin, Q.-Z., Amelin, Y., Stirling, C.H., Kaltenbach, A., 2017. Distribution of ^{26}Al in the CR chondrite chondrule-forming region of the protoplanetary disk. Geochim. Cosmochim. Acta 201, 275-302.

Stracke, A., Palme, H., Gellissen, M., Münker, C., Kleine, T., Birbaum, K., Günther, D., Bourdon, B., Zipfel, J., 2012. Refractory element fractionation in the Allende meteorite: Implications for solar nebula condensation and the chondritic composition of planetary bodies. Geochim. Cosmochim. Acta 85, 114-141.

Trinquier, A., Birck, J.-L., Allègre, C.J., 2007. Widespread ^{54}Cr heterogeneity in the inner solar system. Astrophys. J. 655, 1179-1185.

Trinquier, A., Birck, J.-L., Allègre, C.J., Göpel, C., Ulfbeck, D., 2008. ^{53}Mn-^{53}Cr systematics of the early Solar System revisited. Geochim. Cosmochim. Acta 72, 5146-5163.

van Kooten, E.M.M.E., Wielandt, D., Schiller, M., Nagashima, K., Thomen, A., Larsen, K.K., Olsen, M.B., Nordlund, A., Krot, A.N., Bizzarro, M., 2016. Isotopic evidence for primordial molecular cloud material in metal-rich carbonaceous chondrites. Proc. Natl. Acad. Sci. USA 113, 2011-2016.

Wänke, H., Dreibus, G., 1988. Chemical composition and accretion history of terrestrial planets. Philos. Trans. R. Soc. Lond., Ser. A 325, 545-557.

Wasserburg, G.J., Wimpenny, J., Yin, Q.-Z., 2012. Mg isotopic heterogeneity, Al-Mg isochrons, and canonical $^{26}Al/^{27}Al$ in the early solar system. Meteorit. Planet. Sci. 47, 1980-1997.

Weisberg, M.K., Prinz, M., Clayton, R.N., Mayeda, T.K., Grady, M.M., Pillinger, C.T., 1995. The CR chondrite clan. Proc. NIPR Symp. Antarct. Meteorites 8, 11-32.

Young, E.D., Galy, A., 2004. The isotope geochemistry and cosmochemistry of magnesium. Rev. Min. Geochem. 55, 197-230.

Young, E.D., Shahar, A., Nimmo, F., Schlichting, H.E., Schauble, E.A., Tang, H., Labidi, J., 2019. Near-equilibrium isotope fractionation during planetesimal evaporation. Icarus 323, 1-15.

Tables

Table 1. Mg isotopic compositions of extraterrestrial samples measured at > 2 nA of signal on mass 24 together with bulk Al/Mg ratios. The uncertainties on Δ'^{26}Mg are 2se, but the uncertainties on δ^{26}Mg and δ^{25}Mg are expressed as 2sd to be more representative of the uncertainties when determining δ^{26}Mg and δ^{25}Mg using a bracketing procedure. Typical uncertainties on atomic ^{27}Al/^{24}Mg are better than 1% (2sd).

	Source	Identification Number	Weight (mg)	δ^{26}Mg (‰)	2sd (‰)	δ^{25}Mg (‰)	2sd (‰)	Δ'^{26}Mg (ppm)	2se (ppm)	n	^{27}Al/^{24}Mg
Allende (CV3)	NHM	BM 1988.M24	60.41	-0.281	0.059	-0.155	0.031	22.0	3.0	21	0.1689
Orgueil (CI1)	NHM	BM 36104	98.14	-0.245	0.055	-0.126	0.032	2.1	2.8	33	0.1010
Ivuna (CI1)	NHM	BM 1991, M5	11.6	-0.297	0.025	-0.154	0.010	4.1	2.1	43	0.1024
Alais (CI1)	NHM	BM 1985, M146	4.7	-0.270	0.023	-0.139	0.018	2.8	2.0	43	0.0999[1]
Murchison (CM2)	NHM	BM 1970,6	86.92	-0.321	0.051	-0.168	0.030	7.8	2.8	33	0.1069
Kainsaz (CO3.2)	NHM	BM 1988,M24	69.34	-0.330	0.039	-0.172	0.022	6.2	3.1	33	0.1013
Karoonda (CK4)	NHM	BM 1931, 489	77.54	-0.351	0.061	-0.184	0.033	9.2	1.9	51	0.1168
Renazzo (CR2)	NHM	BM 41105	4.4	-0.364	0.015	-0.183	0.008	-5.5	1.6	44	0.1006
Al Rais (CR2-an)	NHM	BM 1971, 289	4.6	-0.266	0.023	-0.134	0.017	-4.5	2.4	41	0.1074
Abee (EH4)	NHM	BM 1997, M7	66.7	-0.449	0.097	-0.230	0.051	2.0	2.0	33	0.0907
Indarch (EH4)	NHM	BM 1921, 23	97.0	-0.340	0.054	-0.175	0.028	1.4	1.6	39	0.0878
St Mark's (EH5)	NHM	BM 1990, 339	60.37	-0.332	0.070	-0.169	0.042	-1.7	2.6	39	0.0758
Khairpur (EL6)	NHM	BM 51366	69.39	-0.343	0.044	-0.174	0.032	-3.3	3.1	33	0.0741
Hvittis (EL6)	NHM	BM 86754	45.8	-0.308	0.060	-0.157	0.033	-0.1	1.8	30	0.0804
Yilmia (EL6)	NHM	BM 1972, 132	29.8	-0.235	0.071	-0.119	0.038	-2.0	1.7	48	0.0843
Zag* (H3-6)	Meteorite dealer	-	7.18	-0.341	0.053	-0.174	0.029	-1.4	2.7	27	0.0859
Ceniceros (H3.7)	NHM	BM 1989,M31	46.93	-0.327	0.052	-0.165	0.027	-5.3	2.1	31	0.0864
Parnallee (LL3.6)	NHM	BM 34792	6.37	-0.357	0.044	-0.180	0.024	-4.8	3.3	18	0.0863
ALHA 77005* (Shergottite)	NASA	ALHA77 005, 234	71.99	-0.254	0.032	-0.128	0.019	-3.8	2.2	44	
LAR 06319* (Shergottite)	NASA	LAR 06 319, 59	95.58	-0.219	0.078	-0.111	0.043	-2.3	1.7	44	
MIL 03346* (Nakhlite)	NASA	MIL 03 346, 215	84.43	-0.130	0.068	-0.064	0.033	-5.7	1.9	45	
Zagami* (Shergottite)	Meteorite dealer	-	61	-0.231	0.053	-0.116	0.030	-4.7	1.7	45	

* Samples marked with an asterisk were initially homogenised powders, while all the other samples were pieces of meteorites.

[1] The Al/Mg of Alais comes from a different batch of measurements (using a different bracketing standard and an Apex HF introduction system). Given there was no solution left to remeasure it with our latest method, its Al/Mg has been recalculated using the consistent offset obtained for the other samples between the two batches of measurements. This value is given as an informative value only and has not been used to calculate the mean Al/Mg of our CIs.

Table 2. Compilation of the different best-fit regressions discussed in this study.

	$(^{26}Al/^{27}Al)_0$, 2se	$(\Delta'^{26}Mg)_0$	MSWD
CAIs*-CC except CR	$(5.33\pm0.04)\times10^{-5}$	-36.5 ± 1.4 ppm	5.8
OC-CC except CR	$(4.67\pm0.78)\times10^{-5}$	-31.6 ± 5.7 ppm	4.9
ECs only	$(3.75\pm2.09)\times10^{-5}$	-22.7 ± 13 ppm	1.2

* We consider only the high precision datasets of Jacobsen et al. (2008) and Larsen et al. (2011) for CAIs.

95% confidence intervals are calculated by multiplying the *a priori* uncertainties of the York regression by the square root of the MSWD and by the *t*-distribution critical value at 95% confidence.

Figure captions

1) Theoretical precision on Δ'^{26}Mg as a function of acquisition time for various signal intensities. Measured uncertainties are also shown for comparison (blue diamonds for this study, blue circles for Larsen et al. (2011)). The open circle shows the modeled uncertainties for the conditions of measurements (signal intensity and total duration) described in Bizzarro et al. (2011) and the other papers from the StarPlan (Copenhagen) group (the arrow down denotes that the authors only reported a *minimum* signal intensity of 1 nA).

2) The Δ'^{26}Mg of the terrestrial standards measured in this study (BHVO-2, BIR-1, JP-1 and San Carlos olivine; filled symbols). The mean Δ'^{26}Mg is 0.8 ± 2.8 ppm (2se, n = 97) (dashed line and grey area). Literature data (open symbols) are consistent with those of this study.

3) a. Al/Mg isochron plot for bulk chondrites, including our data (filled symbols) and the literature data (open symbols). The best-fit through all bulk ordinary and carbonaceous chondrites except CRs (see text for details) defines an isochron yielding a $(^{26}Al/^{27}Al)_0$ of $(4.67 \pm 0.78)\times10^{-5}$ and an intercept $(\Delta'^{26}Mg_{DSM\text{-}3})_0$ of -31.6 ± 5.7 ppm (calculated using the Isoplot v3 software, Ludwig 2003). Data are from this study, Larsen et al. (2011, 2016), van Kooten et al. (2016) and Schiller et al. (2010). Uncertainties on the regression correspond to the 95% confidence intervals and are calculated by multiplying the *a priori* uncertainties of the York regression by the square root of the MSWD and by the *t*-distribution critical value at 95% confidence.

b. A close-up of the lower part of the a) showing estimates of planetary compositions of the Earth and Mars against chondrite samples shown in a) averaged by petrographic group. Bulk Earth lies clearly to the right of bulk meteorite data. The average Δ'^{26}Mg of the Earth

and Mars are calculated from analyses of this study only, while their Al/Mg ratio are from Palme and O'Neill (2003) and Sanloup et al. (1999), respectively. The bulk Al/Mg of Mars is poorly constrained; here we used the 55% ordinary chondrites (H) + 45% enstatite chondrites (EH) mixture reported by Sanloup et al. (1999) to reproduce the oxygen isotopic composition of Mars. The regression shows a best-fit to all carbonaceous chondrites plotted in a) (other than CRs) and CAIs (Jacobsen et al., 2008; Larsen et al., 2011) to illustrate that the ordinary chondrites plot on a back-projection of this line. This implies CAIs, carbonaceous and ordinary chondrites have common canonical $(^{26}Al/^{27}Al)_0 \approx 5.3\times10^{-5}$ and $(\Delta'^{26}Mg_{DSM\text{-}3})_0 \approx$ -36 ppm.

4) a. Effect of CAI addition to a CI bulk composition. Using the CAI composition labeled with the number 1 on Fig. 4b), we modeled the Al/Mg ratio and Δ'^{26}Mg compositions expected for CAI addition in different proportions by mass (black marks along brown, dashed line) to a CI starting composition (black star). These mixing lines show that the variability within carbonaceous chondrites can be easily explained by their range in CAI content.

b. Comparison between bulk Ca-, Al-rich inclusions (CAIs, dots), hibonites (grey squares) and bulk chondrite (blue box) compositions on an Al-Mg isochron diagram. Note that for CAIs, we consider only Jacobsen et al. (2008, green dots) and Larsen et al. (2011, orange dots) high precision datasets. For the CAIs from Jacobsen et al. (2008), we considered only the ones that were included by the authors in their own best-fit, and rejected the ones that the authors considered as 'altered'. Hibonite data are from Liu et al. (2012). Note that we plot here only the less radiogenic hibonites which are in the range of CAIs.

5) ε^{54}Cr vs Δ'^{26}Mg plot for all bulk chondrite data available in the literature with a precision better than 3 ppm (2se) on Δ'^{26}Mg. There is no correlation between the different groups of carbonaceous chondrites, and only a very weak co-variation between ordinary chondrites,

enstatite chondrites and carbonaceous chondrites. Note that we use the ε^{54}Cr data from Trinquier et al. (2007) to plot our Δ'^{26}Mg data. Refer to the legend of Fig. 3 for the key to the symbols.

6) Simple model of instantaneous fractionation of Al/Mg, from chondritic to planetary value, for the Earth (dashed line), with its uncertainty envelop (solid lines), assuming an enstatite chondrite protolith and a canonical $(^{26}Al/^{27}Al)_0$. The increase in Al/Mg must have occurred 1 Ma after CAIs at the earliest, to generate an Earth with Δ'^{26}Mg in the observed range (shaded area).

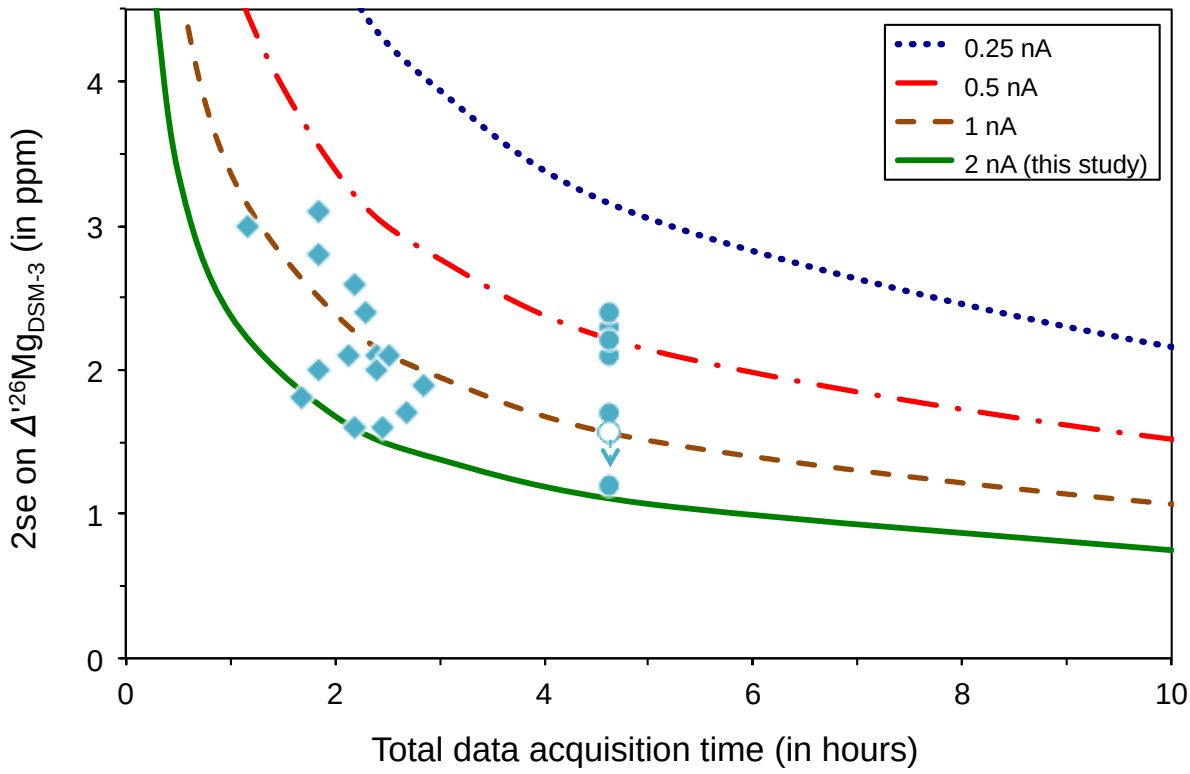

77

78

79 FIGURE 1

80

81

82

83

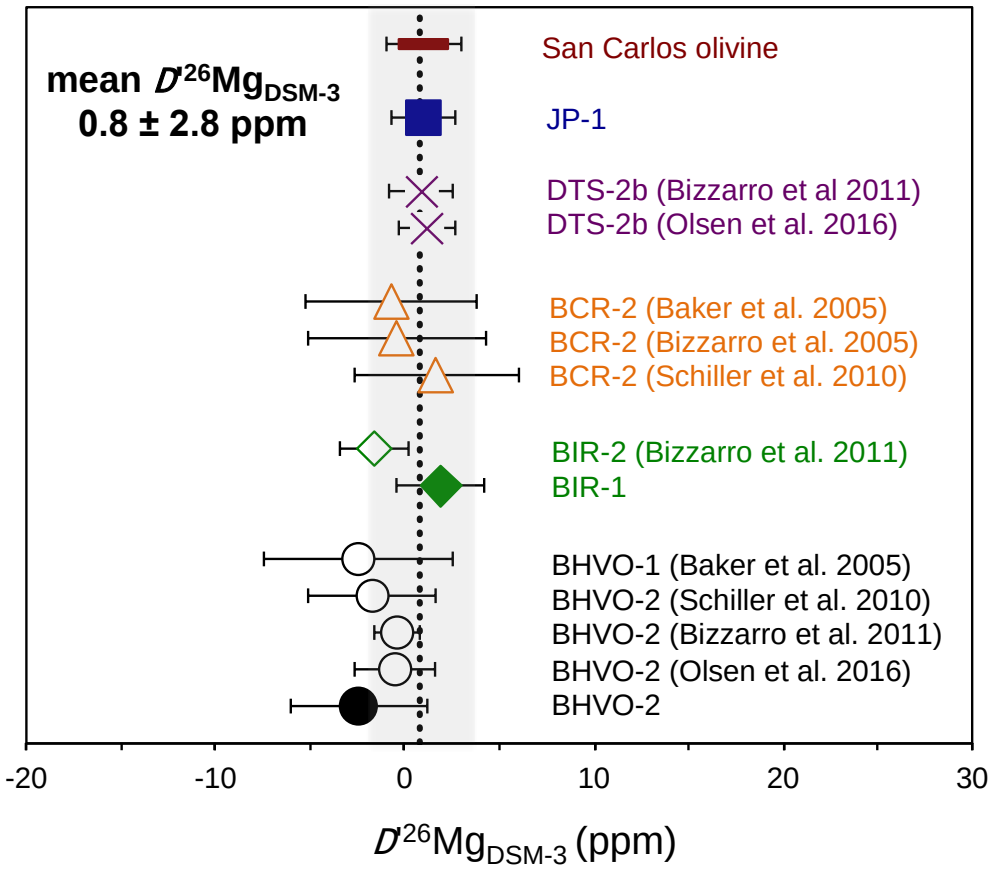

84
85
86 FIGURE 2
87

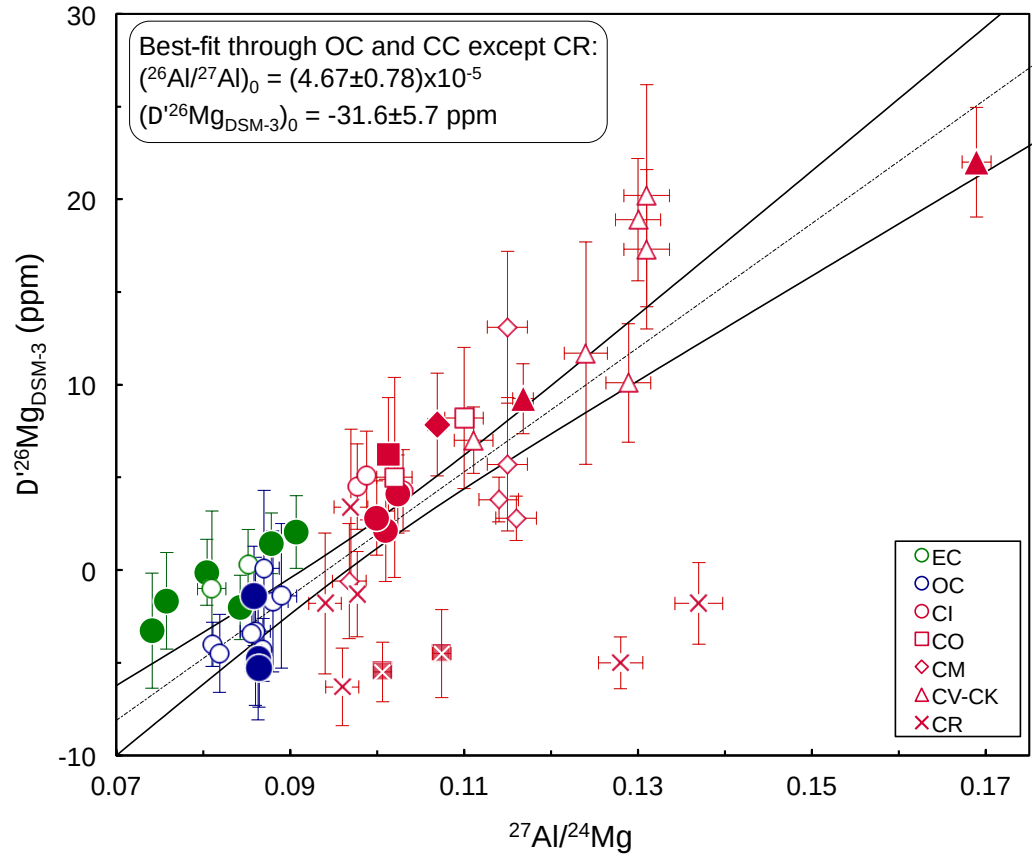
Best-fit through OC and CC except CR:
$(^{26}Al/^{27}Al)_0$ = (4.67±0.78)x10^{-5}
$(D'^{26}Mg_{DSM-3})_0$ = -31.6±5.7 ppm
EC
OC
CI
CO
CM
CV-CK
CR
$D'^{26}Mg_{DSM-3}$ (ppm)
$^{27}Al/^{24}Mg$
30
20
10
0
-10
0.07
0.09
0.11
0.13
0.15
0.17

A.

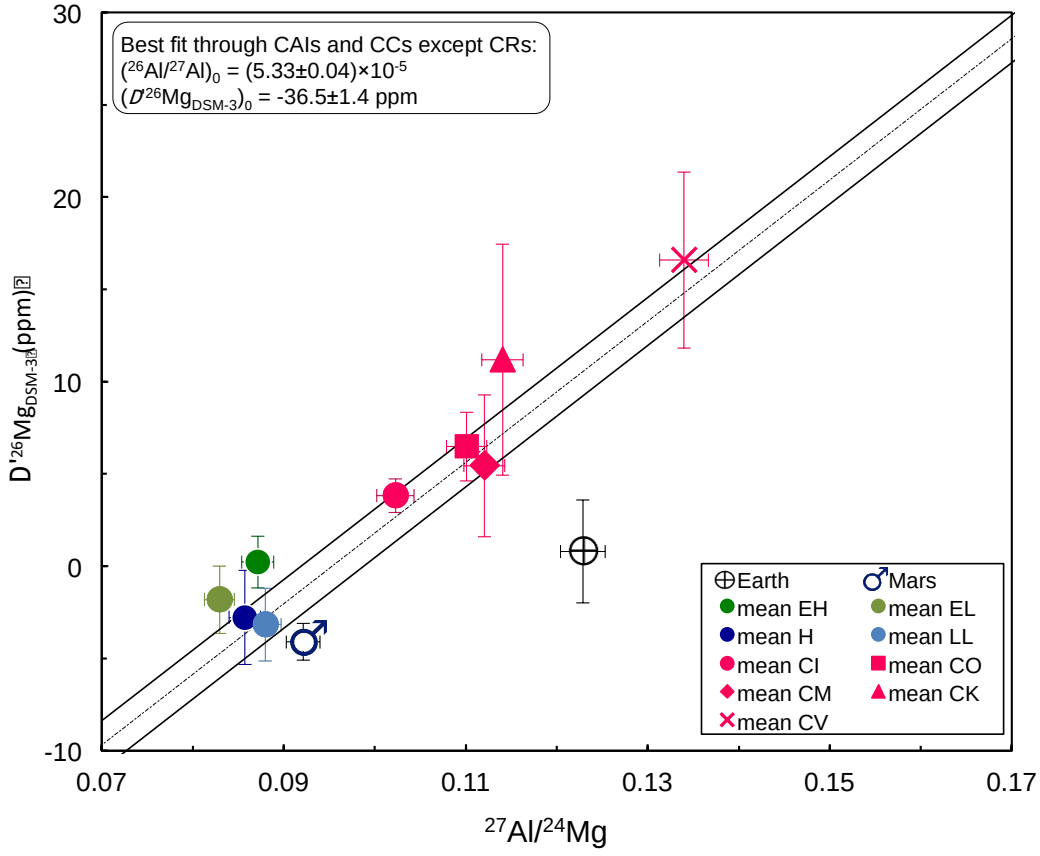
Best fit through CAIs and CCs except CRs:
$(^{26}Al/^{27}Al)_0$ = (5.33±0.04)×10^{-5}
$(D'^{26}Mg_{DSM-3})_0$ = -36.5±1.4 ppm
Earth
Mars
mean EH
mean EL
mean H
mean LL
mean CI
mean CO
mean CM
mean CK
mean CV
$D'^{26}Mg_{DSM-3}$ (ppm)
$^{27}Al/^{24}Mg$
30
20
10
0
-10
0.07
0.09
0.11
0.13
0.15
0.17

B.

FIGURE 3

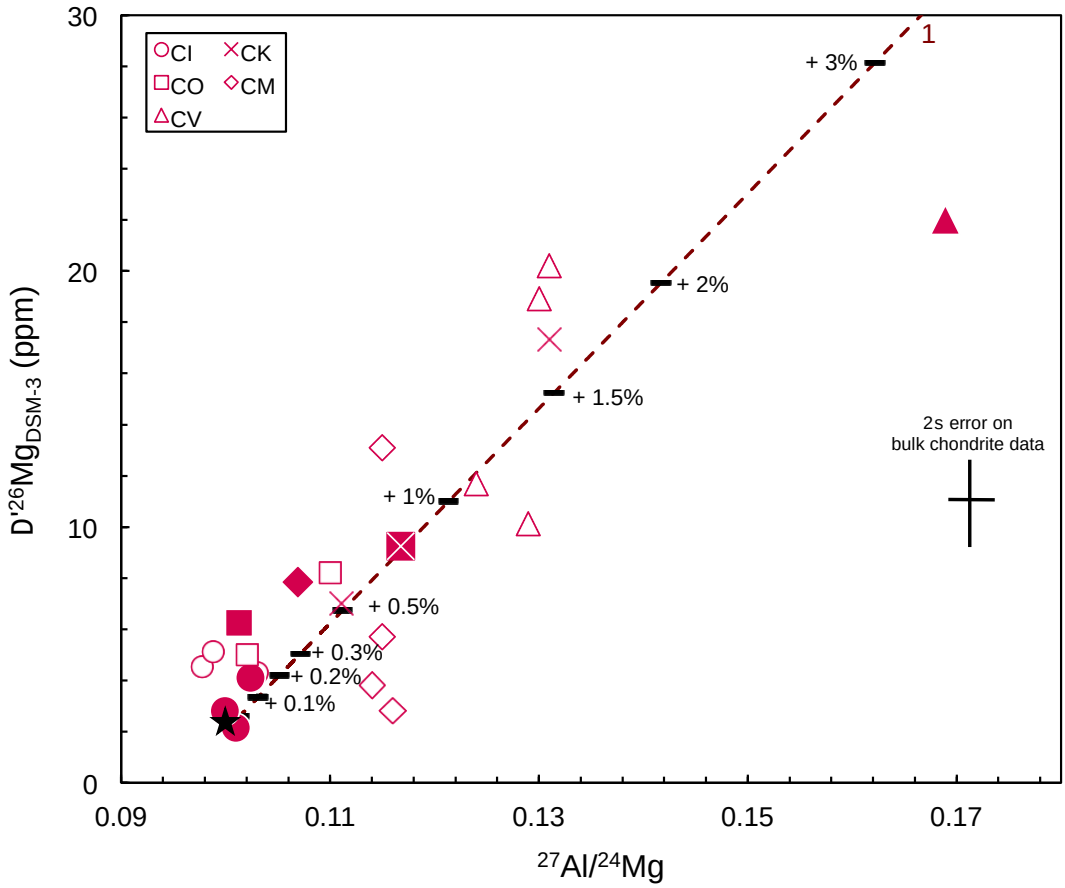
CI
CK
CO
CM
CV
+ 3%
1
+ 2%
+ 1.5%
+ 1%
+ 0.5%
+ 0.3%
+ 0.2%
+ 0.1%
2s error on
bulk chondrite data
D'26MgDSM-3 (ppm)
27Al/24Mg
30
20
10
0
0.09
0.11
0.13
0.15
0.17

A.

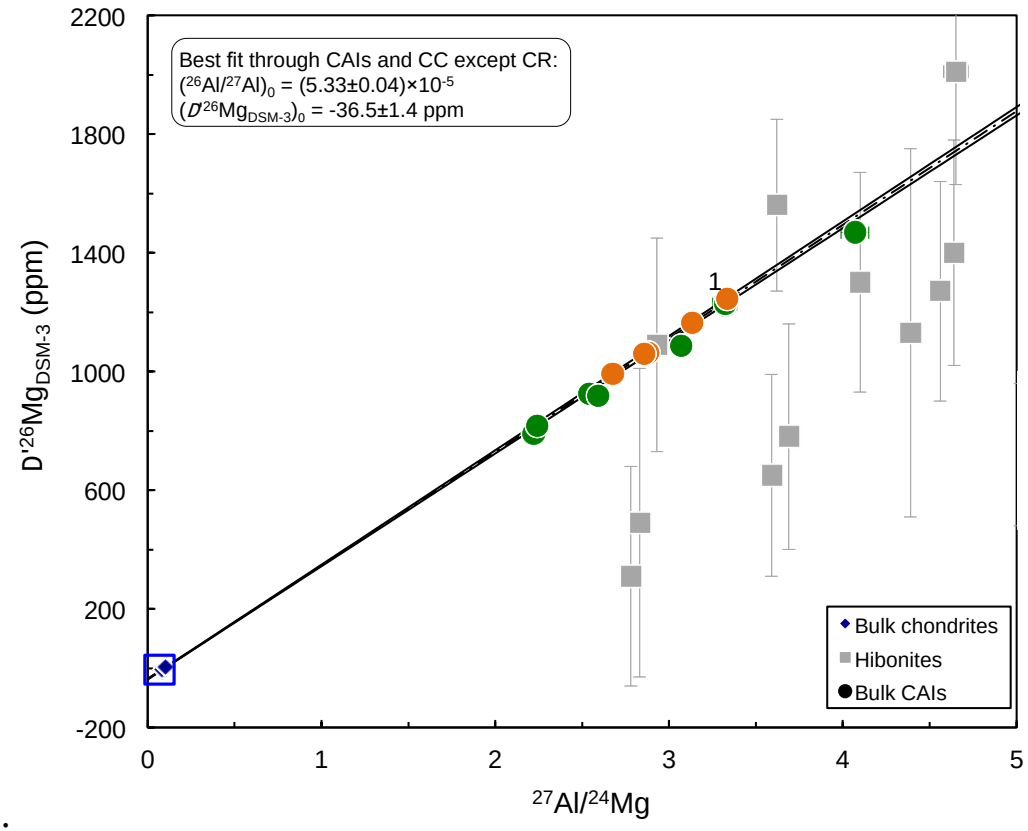
Best fit through CAIs and CC except CR:
(26Al/27Al)0 = (5.33±0.04)×10-5
(D'26MgDSM-3)0 = -36.5±1.4 ppm
1
Bulk chondrites
Hibonites
Bulk CAIs
D'26MgDSM-3 (ppm)
27Al/24Mg
2200
1800
1400
1000
600
200
-200
0
1
2
3
4
5

B.

FIGURE 4

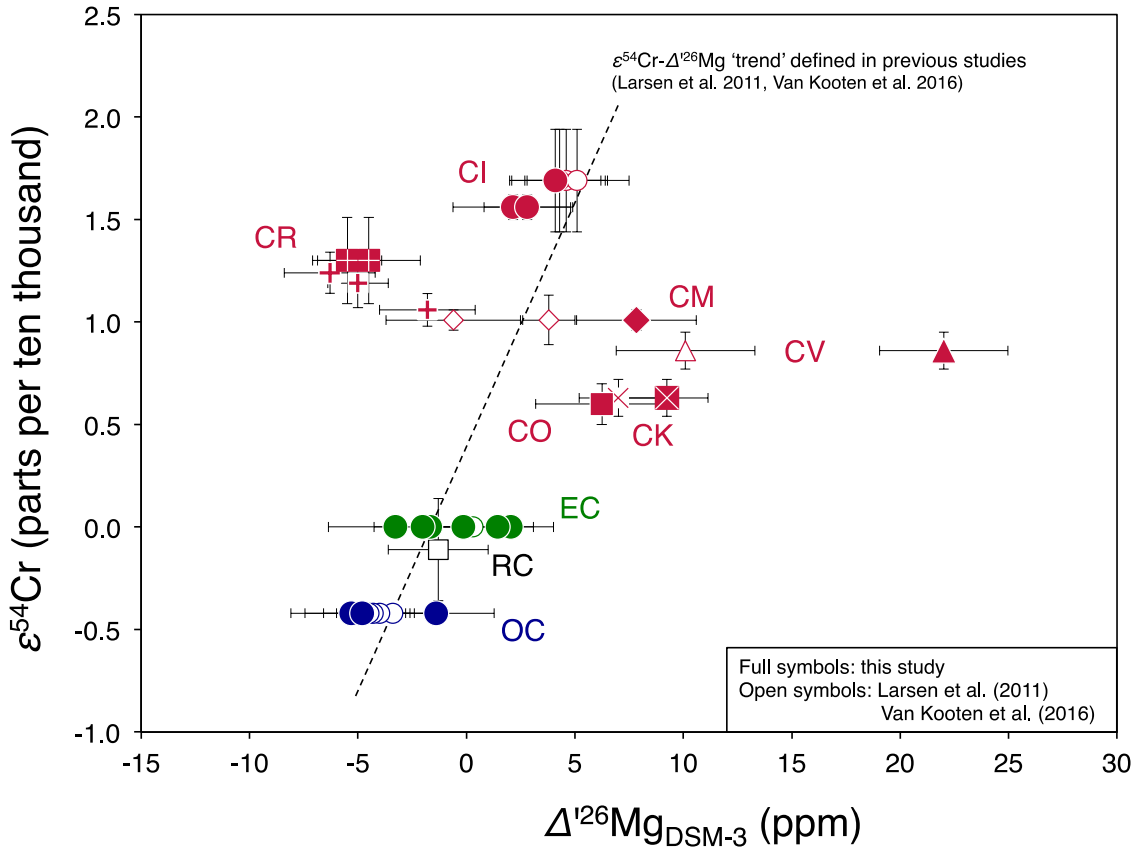
ε54Cr-Δ'26Mg 'trend' defined in previous studies
(Larsen et al. 2011, Van Kooten et al. 2016)
CI
CR
CM
CV
CO
CK
EC
RC
OC
Full symbols: this study
Open symbols: Larsen et al. (2011)
Van Kooten et al. (2016)
ε54Cr (parts per ten thousand)
Δ'26MgDSM-3 (ppm)
2.5
2.0
1.5
1.0
0.5
0.0
-0.5
-1.0
-15
-10
-5
0
5
10
15
20
25
30

FIGURE 5

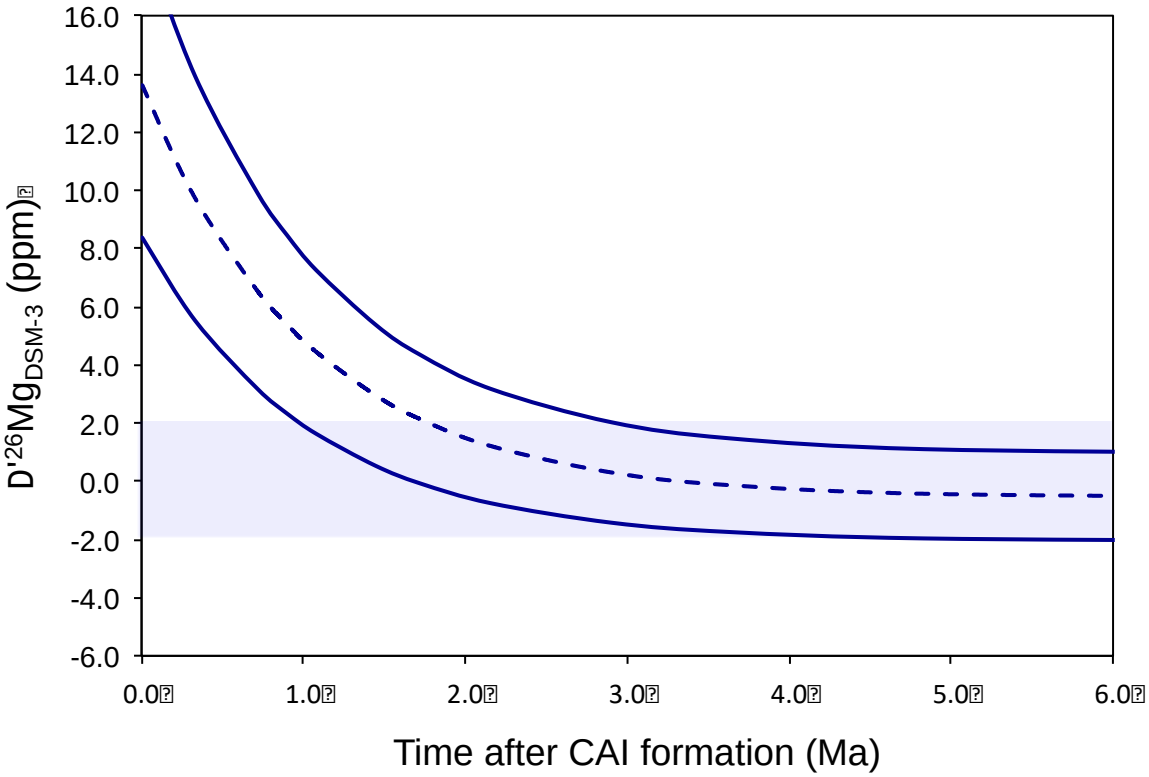

101
102
103 FIGURE 6